

Warped kinematics of the Milky Way revealed by *Gaia*

E. Poggio,^{1,2*} R. Drimmel,² M. G. Lattanzi,² R. L. Smart,² A. Spagna,²
 R. Andrae,³ C. A. L. Bailer-Jones,³ M. Fouesneau,³ T. Antoja,⁴ C. Babusiaux,^{5,7}
 D. W. Evans,⁶ F. Figueras,⁴ D. Katz,⁷ C. Reylé,⁸ A. C. Robin,⁸
 M. Romero-Gómez,⁴ and G. M. Seabroke⁹

¹ *Università di Torino, Dipartimento di Fisica, via P. Giuria 1, I-10125, Torino, Italy*

² *Osservatorio Astrofisico di Torino, Istituto Nazionale di Astrofisica (INAF), I-10025 Pino Torinese, Italy*

³ *Max Planck Institute for Astronomy, Königstuhl 17, D-69117 Heidelberg, Germany*

⁴ *Institut de Ciències del Cosmos, Universitat de Barcelona (IEEC-UB), Martí i Franquès 1, E-08028 Barcelona, Spain*

⁵ *Univ. Grenoble Alpes, CNRS, IPAG, 38000 Grenoble, France*

⁶ *Institute of Astronomy, University of Cambridge, Madingley Road, Cambridge CB3 0HA, UK*

⁷ *GEPI, Observatoire de Paris, Université PSL, CNRS, 5 Place Jules Janssen, 92190 Meudon, France*

⁸ *Institut UTINAM, CNRS UMR6213, Univ. Bourgogne Franche-Comté, OSU THETA Franche-Comté-Bourgogne, Observatoire de Besançon, BP .*

⁹ *Mullard Space Science Laboratory, University College London, Holmbury St Mary, Dorking, Surrey RH5 6NT, United Kingdom*

Accepted XXX. Received YYY; in original form ZZZ

ABSTRACT

Using 2MASS photometry of *Gaia* DR2 sources, we present a technique for selecting upper main sequence stars and giants without the need for individual extinction estimates, to a distance of 7 kpc from the Sun. The spatial distribution of the upper main sequence stars clearly shows the nearest spiral arms, while the large-scale kinematics of the two populations perpendicular to the Galactic plane both show for the first time a clear signature of the warp of the Milky Way.

Key words: Galaxy: kinematics and dynamics – Galaxy: disc – Galaxy: structure – stars: kinematics and dynamics

1 INTRODUCTION

The disc of our Galaxy was first seen to be warped in the radio observations of neutral hydrogen more than 60 years ago (Kerr 1957). Later observations of dust and stars (Freudenreich et al. 1994; Drimmel & Spergel 2001; López-Corredoira et al. 2002; Robin et al. 2008; Reylé et al. 2009; Amôres et al. 2017, and others) also showed that the disc is flat out to roughly the Solar Circle, then bends up upwards in the north and downwards in the south, with the Sun close to the line of nodes.

Warping of stellar discs is also seen in ~50-73% of spiral galaxies (Sanchez-Saavedra et al. 1990; Saha et al. 2009; Ann & Park 2006), which implies that warps are either long lived or are frequently induced. Numerous proposals for the physical cause of warping include interactions with satellites (Kim et al. 2014), intergalactic magnetic fields (Battaner et al. 1990), and a mis-aligned dark halo (Debattista & Sellwood 1999; Sparke & Casertano 1988), amongst others. The fact that not all spiral galaxies are warped, implies

warps are not an intrinsic product of the formation process, and the lack of correlation between the frequency of warps and age (Ann & Park 2006) indicates they are not due to evolutionary effects.

Our Milky Way presents the opportunity for a unique case study of galactic warps. However, to date only the shape of the Galactic warp has been roughly constrained, leading to a lack of consensus for its causal mechanism due to the lack of kinematic information perpendicular to the galactic disc. Since the availability of precise all-sky absolute astrometry, numerous attempts to detect the kinematic signature of the warp have been made (Smart et al. 1998; Drimmel et al. 2000; López-Corredoira et al. 2014; Poggio et al. 2017), though all have been inconclusive. Dehnen (1998) claimed to see the warp using Hipparcos astrometry only, but Seabroke & Gilmore (2007) noted that when radial velocities were included the signature was not convincing. The recent second *Gaia* data release (hereafter *Gaia* DR2), with parallaxes and proper motions significantly more precise than those previously available, and with two orders of magnitude more objects, provides a new opportunity to detect a kinematic warp signature and constrain possible mechanisms. A first kine-

* E-mail: poggio@oato.inaf.it

matic mapping of the Galactic disc with *Gaia* DR2 is given in [Gaia Collaboration et al. \(2018\)](#) (hereafter MWDR2). In this contribution we present a technique to select a larger sample of young Upper Main Sequence (UMS) stars and older giants from *Gaia* DR2, using 2MASS (2-Micron All Sky Survey, [Skrutskie et al. 2006](#)) photometry (Section 2), and compare the kinematic maps of these two samples (Section 3).

2 DATA SELECTION

To select upper main sequence (UMS) and giants in the Galactic plane ($|b| < 20$ deg) without the need for individual reddening estimates, we use 2MASS photometry for *Gaia* DR2 sources using the cross match table provided by the *Gaia* Archive (<https://archives.esac.esa.int/gaia>), and restricting ourselves to 2MASS sources with uncertainties $\sigma_{J,H,K_s} < 0.05$ mag and a photometric quality flag of "AAA". Finally, as a practical matter, we select stars with $G < 16$ mag, as very few fainter stars have 2MASS photometry.

Upper Main Sequence stars. A preliminary selection is made based only on measured 2MASS/*Gaia* colours. As shown in Figure 1, known OB stars from the Tycho-2 Spectral Type Catalogue (hereafter T2STC, [Wright et al. 2003](#)) lie along a sequence that is a consequence of interstellar reddening, which is clearly separated from the redder turn-off stars, giants and lower main sequence stars. Based on this, UMS stars are selected from the *Gaia* DR2∩2MASS catalogue satisfying both $(J - H) < 0.14(G - K_s) + 0.02$ and $(J - K) < 0.23(G - K_s)$.

A second step of the selection procedure uses *Gaia* astrometry ([Lindegren et al. 2018](#)), choosing those stars whose parallax and apparent G magnitude is likely to be consistent with being a UMS star. To this end we calculated the probability density function (pdf) for the heliocentric distance r taking into account the uncertainties on measured parallax, using a prior which assumes an exponential scale height and an exponential fall-off with heliocentric distance (similarly to that suggested by [Bailer-Jones 2015](#); [Astraatmadja & Bailer-Jones 2016a,b](#))

$$P(r|b) \propto \begin{cases} r^2 e^{-|r \sin b|/h_z} e^{-(r \cos b)/L_{rp}}, & \text{if } r > 0 \\ 0, & \text{otherwise} \end{cases} \quad (1)$$

having two different scale lengths perpendicular and parallel to the Galactic plane. For our UMS selection we assume $h_z = 150$ pc and $L_{rp} = 3.5$ kpc. Our choice for h_z here is larger than the known scale height for OB stars ([Poggio et al. 2017](#)), but is such to remove only the stars whose parallaxes and apparent magnitudes are obviously not consistent with the star being an UMS star, though not so small as to condition the distribution of selected stars on the sky. According to Bayes' theorem, the pdf of the heliocentric distance is the posterior $P(r|b, \varpi, \sigma_\varpi) \propto P(r|b)P(\varpi|r, \sigma_\varpi)$, where the adopted prior is shown in Equation 1 and the likelihood is gaussian. For each star, we derived from $P(r|b, \varpi, \sigma_\varpi)$ a pdf of the quantity $M' \equiv M_G + A_G = G - 5 \log r_{pc} + 5$, which is the absolute magnitude M_G plus the extinction in the G band of the source. The Jacobian of the transformation dr/dM' can be written when the G magnitude is fixed, so that we

can perform the change of variable as follows

$$P(M'|b, \varpi, \sigma_\varpi, G) = P(r|b, \varpi, \sigma_\varpi) \left| \frac{d(r|G)}{dM'} \right| \quad (2)$$

After numerically imposing the normalization condition $\int_{-\infty}^{+\infty} P(M'|b, \varpi, \sigma_\varpi, G) dM' = 1$, equation 2 allows us to calculate the probability of the star being brighter than the limit M'_{lim} , which is the faintest extinguished magnitude that we are willing to tolerate for an UMS star candidate with an observed $(G - K_s)$ colour.

The tolerance limit M'_{lim} as a function of $(G - K_s)$ was determined using the PARSEC Isochrones¹ ([Bressan et al. 2012](#); [Chen et al. 2014, 2015](#); [Tang et al. 2014](#)) that relates intrinsic stellar parameters (such as effective temperature, intrinsic luminosity, age, etc.) to the expected *Gaia* and 2MASS photometry. We found that a star with $\log(\text{age/yr}) = 6$ and $\log(T_{eff}) = 4.27$ (roughly corresponding to a B3 star) has, for no extinction, $(M_G)_{lim} = -0.663$ and $(G - K_s) = -0.604$. The PARSEC Isochrones web interface provides the corresponding values of M'_{lim} and $(G - K_s)$ when extinction is present, using the extinction curve from [Cardelli et al. \(1989\)](#); [O'Donnell \(1994\)](#) with $R_V = 3.1$. By interpolating the values furnished by the PARSEC synthetic photometry, a tolerance limit M'_{lim} can be set for each star given its measured $(G - K_s)$. Hence we calculate the probability of the star being an UMS star - i.e. brighter than the tolerance limit - by integrating the pdf in Equation 2:

$$p(UMS|b, \varpi, \sigma_\varpi, G) = \int_{-\infty}^{M'_{lim}} P(M'|b, \varpi, \sigma_\varpi, G) dM' \quad (3)$$

which is by definition between 0 and 1. The stars for which $p(UMS|b, \varpi, \sigma_\varpi, G) > 0.5$, are selected, giving us 716 158 UMS stars.

Giant stars. In a similar fashion as the colour-colour selection of the UMS stars, we perform a preliminary selection based on photometry, this time selecting the stars with $(J - H) > 0.14(G - K_s) + 0.02$ and $(J - K_s) > 0.23(G - K_s)$ (see Figure 1), with an additional $(G - K_s) > 1.8$ cut to remove the objects too blue to be considered giant candidates. We then refine the colour-colour selection by adding a filter based on the measured parallax. Given the large number of giants, we can restrict our selection to the stars with $\varpi/\sigma_\varpi > 5$. On the ground of the small parallax uncertainties, the parallax criterium can be reduced to a simple selection $G + 5 \log \varpi + 5 < M'_{lim}$, where the tolerance limit is set as equal to $M'_{lim} = 1.3(G - K_s) - 1.7$. Such a limit removes sub-giants and dwarfs, and also accounts for interstellar reddening (see Figure 2, right plot). This selection gives us 6 560 075 giants.

To test the composition of the selected samples, we crossmatched our samples with the T2STC. For the UMS sample, we obtained 24 422 objects, of which approximately 55% are OB stars, 40% are A stars and 5% are F stars, according to the T2STC spectral classifications. For the giant sample, we found 33 398 stars with complete spectral classification from T2STC, of which 86% are giants (67% K giants and 19% G giants) and 14% are main sequence stars (mostly of spectral class K or G, while A or F stars are less than 1%).

¹ web interface <http://stev.oapd.inaf.it/cmd>

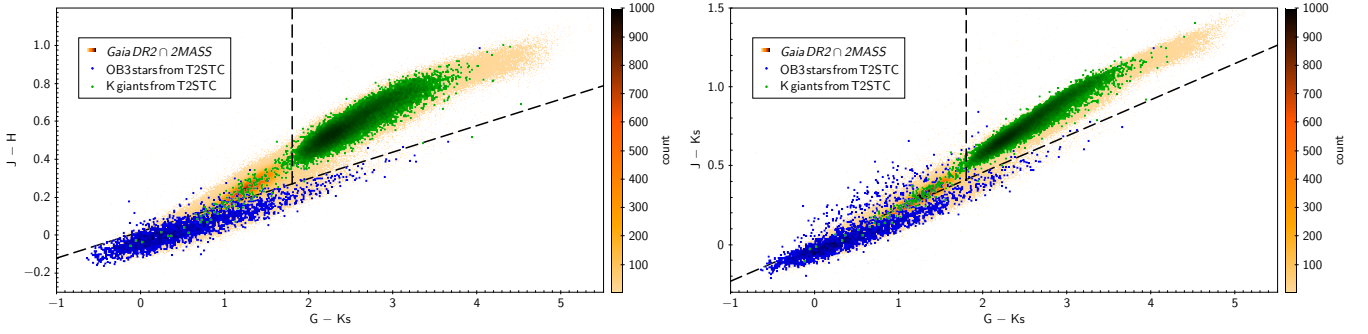


Figure 1. Colour-colour plots showing the 2MASS-*Gaia* colour-colour selection. Candidate upper main sequence (UMS) are taken as stars lying below the diagonal dashed lines, while candidate giant stars are taken as stars lying in the top right area of the plots. The yellow-orange density plots a sample of *Gaia* DR2 stars with $G < 12$ with bins of 0.001 mag, to show where stars of all different types fall in these colour-colour plots, while the blue and green points show the colours of stars in the Tycho-2 Spectral Type Catalogue (T2STC) that are classified as either OB stars or K giants (luminosity class I and II).

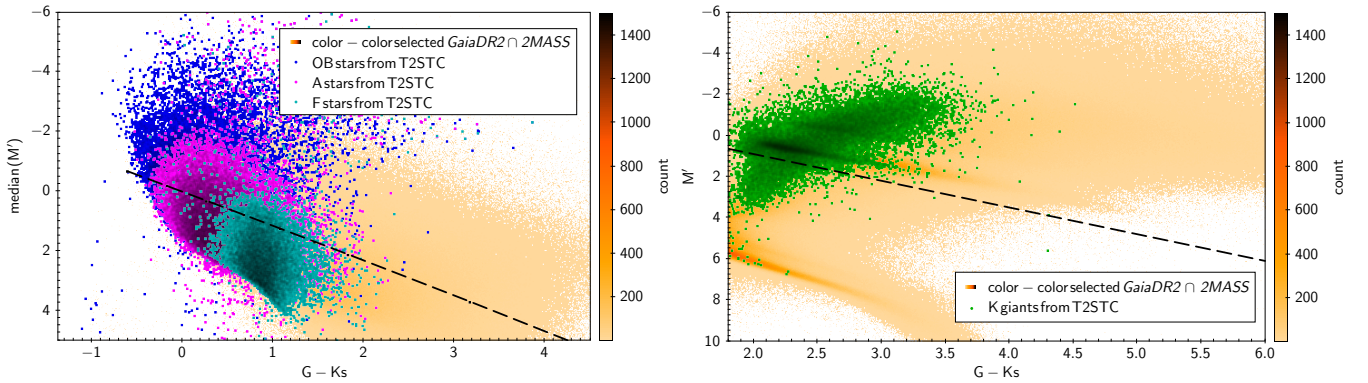


Figure 2. *Left panel:* the parallax criterion for the upper main sequence (UMS) stars. On the y-axis, the median of the probability density function of M' (Equation 2). *Right panel:* the parallax criterion for the giants. On the y-axis, M' calculated as described in the text. The dashed line shows the adopted tolerance limits (see text), selecting those stars that are above the dashed lines. Orange densities area as in the previous plots, other coloured points are for those stars in the Tycho-2 Spectral Type Catalogue (T2STC), colour coded as per the key in the figures.

3 DENSITY AND KINEMATIC MAPS

In this Section, we present and compare the maps obtained with the UMS and giant samples, shown in Figure 3. For both samples we use as our distance estimator for each star the mode of the pdf of the heliocentric distance, $P(r|b, \varpi, \sigma_\varpi)$, that uses the prior in Equation 1, using $h_z = 150$ pc for the UMS sample, and $h_z = 300$ pc (Bland-Hawthorn & Maloney 2002) for the giant sample. (Since the selected giants are constrained to have $\varpi/\sigma_\varpi > 5$, the resulting distribution of distances are nearly identical to assuming $1/\varpi$ as the distance.) Using these distances and the (l, b) coordinate, we determine the heliocentric XY coordinates in the Galactic plane, and bin the stars in 400 pc wide cells. The giant sample exhibits a smooth density distribution (top right plot), decreasing for large heliocentric distance, as expected for a magnitude limited sample, and for larger Galactocentric radii, as expected from an exponential disc. In contrast the UMS sample (top left plot) shows three observed overdensities that corresponds to sections of the nearby spiral arms (from left to right: Sagittarius-Carina arm, local arm and Perseus arm). The evident spiral struc-

ture confirms that our UMS sample is young with respect to the smooth distribution shown by the older and dynamically relaxed giant population.

The proper motions perpendicular to the Galactic plane, μ_b , are derived from the *Gaia* DR2 astrometry. These proper motions are dominated by the reflex of the solar motion, producing large negative values for stars near the Sun. In order to compensate for this effect, we corrected the proper motions μ_b for the Solar motion (second row of Figure 3), assuming $(V_{x\odot}, V_{y\odot}, V_{z\odot}) = (11.1, 12.24, 7.25)$ km s $^{-1}$ (Schönrich et al. 2010). Both samples already show a significant increase of the proper motion toward larger Galactocentric radii, in agreement with the expectation from kinematic models of the Galactic warp (Abedi et al. 2014; Poggio et al. 2017). Radial features in this plot are due to uneven sampling above/below the Galactic plane due to foreground extinction.

The large majority of stars in our UMS sample lack line-of-sight velocities so that it is not possible to calculate directly the vertical velocity. We therefore estimate the mean vertical velocity V_z^2 from the available astrometry, correcting for solar motion and differential Galactic rotation, assuming

a flat rotation curve, as done in MWDR2. For the giants we find that 37% have line-of-sight velocities provided in *Gaia* DR2, for which we calculate directly the vertical velocity, while for the remaining we estimate the vertical velocities as done for the UMS sample.

On large scales the velocity maps of our two samples are quite similar, showing positive velocities at large Galactocentric radii, as expected from the warp. There are still some differences on small scales, perhaps inherited from the gas. Also worthy to note is that the peak velocities in both samples is not exactly toward the anti-center, which might be due to the Sun not being on the line-of-nodes.

4 DISCUSSION AND CONCLUSIONS

The kinematic signature of the Galactic warp is expected to manifest itself toward the Galactic anticenter as large-scale systematic velocities perpendicular to the Galactic plane. Thanks to the large sample of stars in *Gaia* DR2 with exquisite astrometric precision, we are able to map the vertical motions over a larger extent of the Milky Way's disc than previously possible, for both an intrinsically young and old population. That our UMS sample clearly shows the spiral arms, in contrast with the giant population, confirms that it is a dynamically young population.

Most recently MWDR2 made a similar comparison with smaller samples from *Gaia* DR2 over a smaller area of the disc, which showed an apparent discordance in the vertical motions of the young and old stars. Here we find that, while the kinematics of the giant sample is very similar to MWDR2, the UMS sample here shows vertical motions very similar to the giants. This is an important clue to the nature of the Galactic warp, indicating that the mechanism producing the warp must be common to both dynamically young and old stellar populations. Indeed, from these results we can conclude that the warp is a purely gravitational phenomenon, reflecting a warp in the gravitational potential of the outer Milky Way.

We have here only qualitatively evidenced the kinematic signature the warp in *Gaia* DR2. Our findings bear further witness to the great potential of this data set. Future work confronting this signature with more quantitative models will certainly reveal further details of the dynamical nature of the Galactic warp.

ACKNOWLEDGEMENTS

This work has made use of data from the European Space Agency (ESA) mission *Gaia* (<https://www.cosmos.esa.int/gaia>), processed by the *Gaia* Data Processing and Analysis Consortium (DPAC, <https://www.cosmos.esa.int/web/gaia/dpac/consortium>). Funding for the DPAC has been provided by national institutions, in particular the institutions participating in the *Gaia* Multilateral Agreement. This publication makes use of data products from the Two Micron All Sky Survey, which is a joint project of the University of Massachusetts and the Infrared Processing and Analysis Center/California Institute of Technology, funded by the National Aeronautics and Space Administration and the National Science Foundation. This project was

developed in part at the 2016 NYC Gaia Sprint, hosted by the Center for Computational Astrophysics at the Simons Foundation in New York City. E. Poggio acknowledges the financial support of the 2014 PhD fellowship programme of INAF. This work was supported by the MINECO (Spanish Ministry of Economy) through grant ESP2016-80079-C2-1-R (MINECO/FEDER, UE) and MDM-2014-0369 of ICCUB (Unidad de Excelencia 'María de Maeztu').

REFERENCES

- Abedi H., Figueras F., Aguilar L., Mateu C., Romero-Gomez M., Lopez-Corredoira M., Garzon Lopez F., 2014, in EAS Publications Series. pp 237–240, [doi:10.1051/eas/1567042](https://doi.org/10.1051/eas/1567042)
- Amôres E. B., Robin A. C., Reylé C., 2017, *A&A*, **602**, A67
- Ann H. B., Park J.-C., 2006, *New Astron.*, **11**, 293
- Astraatmadja T. L., Bailer-Jones C. A. L., 2016a, *ApJ*, **832**, 137
- Astraatmadja T. L., Bailer-Jones C. A. L., 2016b, *ApJ*, **833**, 119
- Bailer-Jones C. A. L., 2015, *PASP*, **127**, 994
- Battaner E., Florido E., Sanchez-Saavedra M. L., 1990, *A&A*, **236**, 1
- Bland-Hawthorn J., Maloney P. R., 2002, in Mulchaey J. S., Stocke J. T., eds, *Astronomical Society of the Pacific Conference Series Vol. 254, Extragalactic Gas at Low Redshift*. p. 267 ([arXiv:astro-ph/0110044](https://arxiv.org/abs/astro-ph/0110044))
- Bressan A., Marigo P., Girardi L., Salasnich B., Dal Cero C., Rubele S., Nanni A., 2012, *MNRAS*, **427**, 127
- Cardelli J. A., Clayton G. C., Mathis J. S., 1989, *ApJ*, **345**, 245
- Chen Y., Girardi L., Bressan A., Marigo P., Barbieri M., Kong X., 2014, *MNRAS*, **444**, 2525
- Chen Y., Bressan A., Girardi L., Marigo P., Kong X., Lanza A., 2015, *MNRAS*, **452**, 1068
- Debattista V. P., Sellwood J. A., 1999, *ApJ*, **513**, L107
- Dehnen W., 1998, *AJ*, **115**, 2384
- Drimmel R., Spergel D. N., 2001, *ApJ*, **556**, 181
- Drimmel R., Smart R. L., Lattanzi M. G., 2000, *A&A*, **354**, 67
- Freudenreich H. T., et al., 1994, *ApJ*, **429**, L69
- Gaia Collaboration et al., 2018, preprint, ([arXiv:1804.09380](https://arxiv.org/abs/1804.09380))
- Kerr F. J., 1957, *AJ*, **62**, 93
- Kim J. H., Peirani S., Kim S., Ann H. B., An S.-H., Yoon S.-J., 2014, *ApJ*, **789**, 90
- Lindgren L., et al., 2018, preprint, ([arXiv:1804.09366](https://arxiv.org/abs/1804.09366))
- López-Corredoira M., Cabrera-Lavers A., Garzón F., Hammersley P. L., 2002, *A&A*, **394**, 883
- López-Corredoira M., Abedi H., Garzón F., Figueras F., 2014, *A&A*, **572**, A101
- O'Donnell J. E., 1994, *ApJ*, **422**, 158
- Poggio E., Drimmel R., Smart R. L., Spagna A., Lattanzi M. G., 2017, *A&A*, **601**, A115
- Reylé C., Marshall D. J., Robin A. C., Schultheis M., 2009, *A&A*, **495**, 819
- Robin A. C., Reylé C., Marshall D. J., 2008, *Astronomische Nachrichten*, **329**, 1012
- Saha K., de Jong R., Holwerda B., 2009, *MNRAS*, **396**, 409
- Sanchez-Saavedra M. L., Battaner E., Florido E., 1990, *MNRAS*, **246**, 458
- Schönrich R., Binney J., Dehnen W., 2010, *MNRAS*, **403**, 1829
- Seabroke G. M., Gilmore G., 2007, *MNRAS*, **380**, 1348
- Skrutskie M. F., et al., 2006, *AJ*, **131**, 1163
- Smart R. L., Drimmel R., Lattanzi M. G., Binney J. J., 1998, *Nature*, **392**, 471
- Sparke L. S., Casertano S., 1988, *MNRAS*, **234**, 873
- Tang J., Bressan A., Rosenfield P., Slemmer A., Marigo P., Girardi L., Bianchi L., 2014, *MNRAS*, **445**, 4287
- Wright C. O., Egan M. P., Kraemer K. E., Price S. D., 2003, *AJ*, **125**, 359

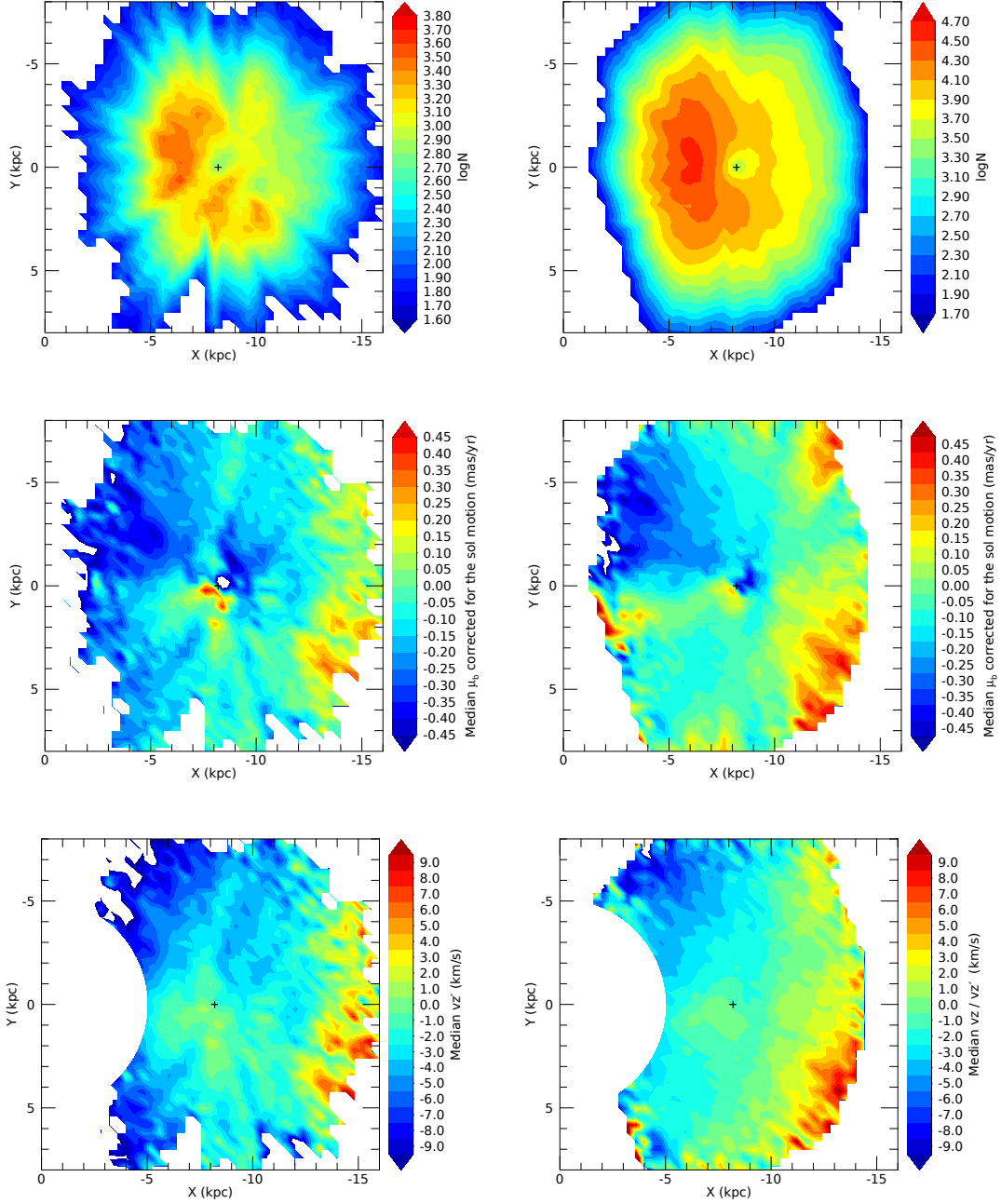


Figure 3. Maps for the UMS (left plots) and giant (right plots) samples. The Sun is represented by a black cross at $X = -8.35$ kpc and $Y = 0$ kpc. The Galactic center is located at $X = 0$ and $Y = 0$, and the Galaxy is rotating clockwise. The XY plane was divided into cells of 400 pc width, only showing the ones containing more than 50 stars. From top to bottom: log-density map (N is the number of sources per cell), μ_b corrected for the Solar motion and V_z' (see text). In the bottom plots, cells with Galactocentric radius < 5 kpc were removed, since the assumed rotation curve cannot describe correctly those cells.

This paper has been typeset from a $\text{\TeX}/\text{\LaTeX}$ file prepared by the author.